Civil Engineering Infrastructures Journal xx,xx
DOI: 10.22059/ceij.2026.393103.2290

Numerical Investigation on the Influence of Shear Lag on Flange Buckling strength of Fiber Reinforced Polymer (FRP) Box Beams

M. Kasiviswanathan[1*], Akhil Upadhyay[2]

[1]Department of Civil Engineering, Sona College of Technology, Salem 636005, India

*Email: kasiviswanathan.civil@sonatech.ac.in

Orchid id: 0000-0002-2824-9065

[2] Department of Civil Engineering, Indian Institute of Technology Roorkee, Roorkee 247667, India

Email: akhilfce@iitr.ac.in

Received: 16/04/2025
Revised: 09/10/2025
Accepted: 29/11/2025

Abstract. The combination of fiber reinforced polymer composite and box-beam is ideal for light weight bridges but being a thin-walled structure, their designs are often governed by buckling criteria. In the FRP box beam, two types of local bucklings are possible i.e. flange and web buckling. In the wide flange box-beam, flange buckling strength is mainly affected by shear lag phenomenon and it becomes more significant in FRP box-beam due to their quasi-brittle material behaviour. Hence, an attempt is made to understand the effect of shear lag on flange buckling strength of FRP box beams. Firstly, the influence of

rotational restraint and moment gradient is desensitized by choosing an appropriate geometry and loading conditions. Similarly, influence of $(b/t)_F$ is isolated by using percentage difference in buckling coefficient by comparing finite element (FE) analysis and closed form equation results. Secondly, parametric study based on the linear elastic buckling analysis is conducted to quantify the influence of shear lag on flange buckling coefficient. Finally, based on the numerical results thus obtained and shear lag parameters ($\omega_{1,mod}$ and k_1), generic curves as well as classes having different range of % increase in buckling coefficient are presented which will be more helpful to the designers.

Keywords: FE analysis, Stability problem, fiber reinforced polymer box-beam, Flange buckling, Shear lag.

1. Introduction

Initially, thin-walled box-beams are widely used in aircraft wings because of their light weight and torsional properties. In bridges, box-beam finds many applications due to their good bending resistance, sectional integrity and better construction adoptability. However, due to the thin-walled configuration of the section, the shear lag phenomenon arises, thereby diminishing the structural efficiency of the section (Moga et al., 2020a, 2021). Further, because of non-uniform stress distribution resulting from shear lag, buckling behaviour of beam also gets affected as it depends on state of stress in elements.

According to elementary bending theory, longitudinal normal stress distribution across the flange width is assumed to be uniform. In contrast, for beams having thin/wider flange, due to shear deformation, longitudinal stress distribution becomes non-uniform across the flange width. The value of stress at web-flange junction is higher than the value of stress remote from the web (Fig. 1). This phenomenon is called shear lag, and it has been studied by many researchers (Von Karman (1924), Li et al. (2019), Singh et al. (2020) and jiang et al. (2023)).

The earliest research for shear lag phenomenon was carried out by Von Karman in 1924. Von Karman (1924) introduced effective width concept (b_e), later, it was widely adopted and followed by many researchers. Priors have used different analytical models and methods to study the shear lag phenomenon such as theorem of least work, energy method (Li et al. (2019), Singh et al. (2020) and jiang et al. (2023)), folded-plate method, bar simulation method, harmonic analysis method, sub-structuring analysis method, spline finite member element method, single Fourier series method, finite segment model, 3-bar simulation-transfer matrix method and energy variational method (Chen et al. (2014)). Li et al. (2019) proposed an improved analytical method to study the shear lag effect in thin-walled box-section beams with varying cantilever flange widths. Their model accounted for flexural–shear coupling and provided better accuracy near the web–flange junctions compared to classical methods. Likewise, Singh et al. (2020) developed a simplified approach to analyze negative shear lag in laminated composite cantilever beams, emphasizing the influence of material anisotropy and stacking sequence. Jiang et al. (2023) examined composite box girders with corrugated steel webs and found that the corrugated geometry helps reduce shear lag by improving shear stiffness and stress distribution across the flanges. Similarly, Chen et al. (2014) proposed a closed-form analytical solution for the shear lag problem in box girders by introducing a derived flange deformation function that accurately represents longitudinal stress variation along the flange width. Their method improved the prediction of stress distribution, particularly near flange–web junctions, compared to conventional models.

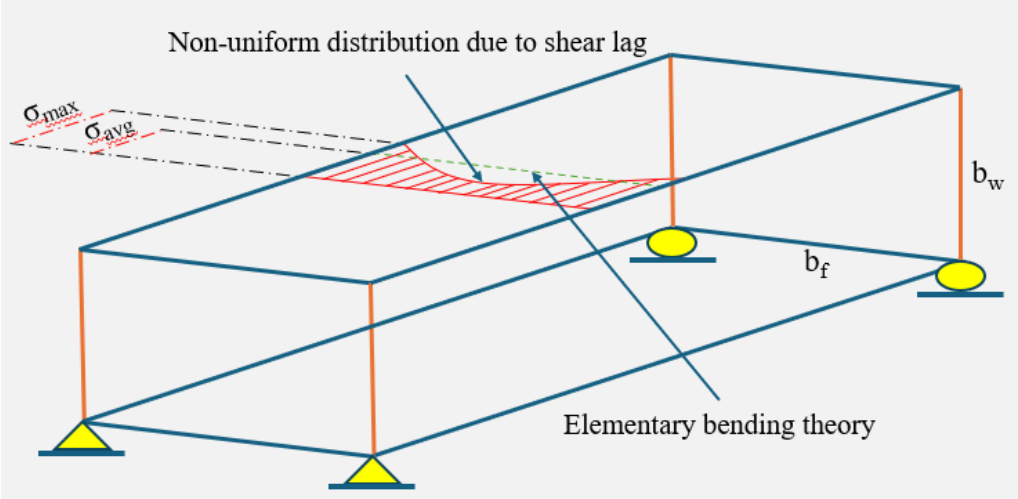

Fig. 1. Longitudinal normal stress distribution across the flange width in simply supported box-beam.

Later, because of increasing applications of fiber reinforced polymer beam in various engineering fields, few researchers have extended some of the above-mentioned analytical models for orthotropic material. For example: single Fourier series, principle of minimum potential energy, three bar analogy (Upadhyay and Kalyanaraman (2003)), harmonic technique (Salim and Davalos (2005)) and effective width concept (Chandak et al. (2008)). Upadhyay and Kalyanaraman (2003) presented a simplified analysis for FRP box girders, highlighting how material orthotropy influences shear lag behavior and demonstrating that FRP girders experience less shear lag due to their high stiffness-to-weight ratio. Salim and Davalos (2005) extended this understanding to both open and closed thin-walled laminated composite beams, showing that laminate orientation significantly affects stress transfer and shear lag magnitude. In addition, Chandak et al. (2008) developed an artificial neural network model to predict shear lag in symmetrical laminated composite box beams, achieving results closely matching analytical and finite element solutions, thereby demonstrating the potential of AI-based approaches in capturing complex shear lag behavior.

FRP offers many advantages over traditional materials (concrete and steel) such as high strength, light weight and design feasibility, hence it has been increasingly applied in structural

engineering research and analysis (Zeinali et al. (2020), Kasiviswanathan and Anbarasu (2021), Nuraliyev et al. (2022), Mohammadizadeh and Esfandnia (2022), Si et al. (2023) and Kilani et al. (2025)). Though, due to their high strength/stiffness ratio, FRP beams often fail by buckling before reaching their ultimate material strength as shown in Fig. 2.

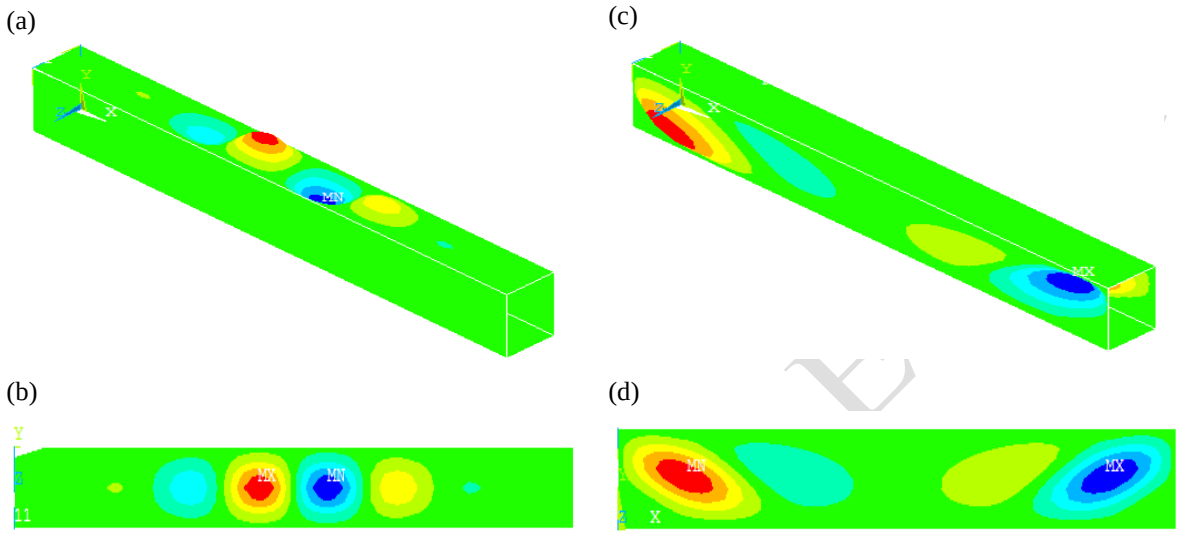

Fig. 2: Buckling mode shape corresponding to the first Eigen value (a, b) Flange buckling - isometric and top view (c, d) Web buckling – isometric and side view.

Buckling depends on state of stress in flange and web elements. Under symmetrical lateral load, state of stress is influenced more by secondary effects such as rotational restraint, moment gradient and shear lag. Effect of stress gradient on buckling of composite plate was studied by Yu and Schafer (2007). Similarly, influence of rotational restraint on buckling of composite plates is studied by Kollar (2003) and Qiao and Shan (2005). Kasiviswanathan and Upadhyay (2018) have studied the influence of various secondary effects on flange buckling coefficient of FRP box beams by FE approach. They found the governing parameters and trends affecting the flange buckling coefficient, but they didn't study the effect of shear lag on flange buckling.

Due to high degree of orthotropy, analytical determination of shear lag influences on buckling capacity of FRP beam is a tedious task. In addition, analytical methods introduce assumption to simplify a model and yield an approximate solution which cannot be reliably

used in design. While finite element (FE) analysis provides accurate/reliable results for FRP composites together with no limitations on boundary and loading condition. Yamaguchi et al. (2008) have studied the influence of shear lag on deflection and stress concentration by using FE analysis.

The literature review indicates that although numerous studies have been carried out on the shear lag phenomenon, most of them focus primarily on deflection and stress distribution. A few researchers have considered the effect of shear lag on beam buckling; however, their investigations were mostly limited to isotropic materials. Due to the presence of multiple variables (i.e. length, thickness, Ply orientation and laminate configurations etc.,), complex stress states, and secondary effects, understanding the influence of shear lag on the flange buckling coefficient of FRP box beams remains a challenging task. At the same time, the use of thin and wide FRP box beams has been steadily increasing in various engineering fields owing to their superior advantages. Therefore, to support better design practices, it is essential to study the buckling behaviour of FRP beams by incorporating shear lag effects. Hence, in this paper, effect of shear lag on flange buckling coefficient of FRP box beams has been studied with the help of shear lag parameters $\omega_{1,\mathrm{mod}}$ and k_1. In addition, an attempt is made to extract trends affecting the flange buckling coefficient by using shear lag parameters which will be helpful for better design.

2. Finite element analysis

FRP box beam comprises of top flange, webs and bottom flange. When flange bends due to lateral load, it will get rotational restrained from web which is not considered in discrete approach. Hence, to replicate the real behaviour of flange and webs, FRP box-beams are modelled and analyzed by using finite element software ANSYS (2003). SHELL281 element from the ANSYS element library is selected to discretize the box beam models. SHELL281 is a 8 noded element, it has both membrane and bending capabilities. The element has 8 nodes

and 6 degrees of freedom per node: translation in the nodal X, Y and Z direction and rotation about X, Y and Z axes. This shell element has successfully been adopted in previous finite element studies in thin-walled pultruded profiles by other researchers (Kadhom et al. (2021), Said et al. (2022) and Shivekar and patil (2023)).

Graphite-epoxy material is used to model the box-beam components (flange and web). Table 1 shows the material mechanical properties of graphite-epoxy. The beam shown in Fig. 3 is used for analysis. To create the hinge support X, Y, Z direction of center node and Y, Z directions of rest of nodes are constrained at one end, similarly, to create roller support Y and Z directions are constrained at the other end.

Table 1. Lamina material properties

E_1 (GPa)	E_2 (GPa)	G_{12} (GPa)	ρ (kg/m^3)	v_{12}	v_{21}
145	16.5	4.48	1520	0.314	0.037

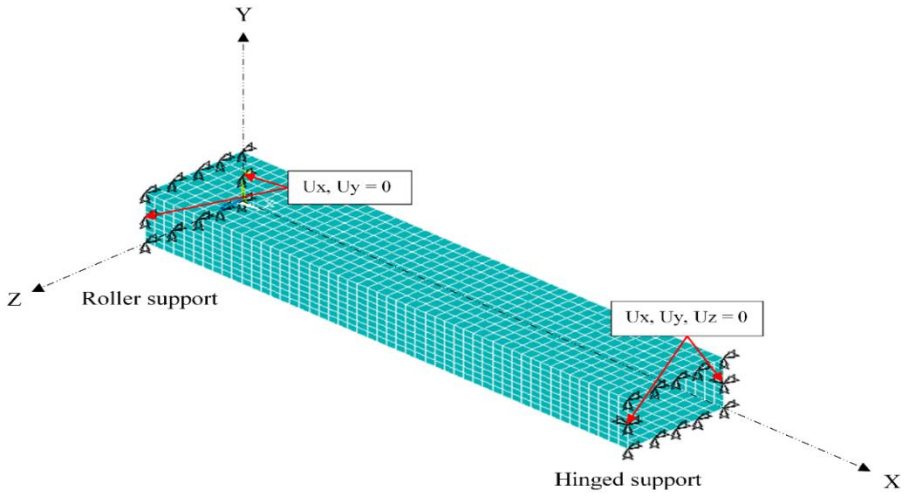

Fig. 3. Discretized beam model with end constraints.

2.1 Beam geometry selection

In all the analysis, flange buckling is kept as the dominant buckling mode. It is achieved by keeping slenderness value of web $(b/t)_w$ lower than flange slenderness value $(b/t)_f$. In this study, minimum b/t value considered for web and flange is 20 and 375, respectively. Three different

flange thicknesses and four different flange widths are used to arrive at these wide range of slenderness ratios. Five laminate configurations are used for both the web and flange to examine the effect of fiber orientation on structural performance. Figure 3. Shows the schematic view of laminate configurations. The selected laminates are $[(0/0)_2]s$, $[(\pm45)_2]s$, $[(90/90)_2]s$, $[(0)_2/(\pm45)]s$, and $[(0)_2/(90)_2]s$. The unidirectional laminate $[(0/0)_2]s$ provides high stiffness and strength in the longitudinal direction, whereas the angle-ply laminate $[(\pm45)_2]s$ is effective in resisting shear and torsional stresses. The transverse laminate $[(90/90)_2]s$ improves transverse stiffness but is less effective in axial loading. The hybrid laminates $[(0)_2/(\pm45)]s$ and $[(0)_2/(90)_2]s$ offer a balance of properties by combining longitudinal, shear, and transverse plies, thereby enhancing overall buckling resistance and stability. These five laminates cover a wide range of behaviors, allowing a comprehensive study of their performance in web- and flange-dominated loading conditions. For all simulations, the length of the beam and width and thickness of the webs are kept constant. The considered laminate configurations and geometry of the beam are shown in Table 2.

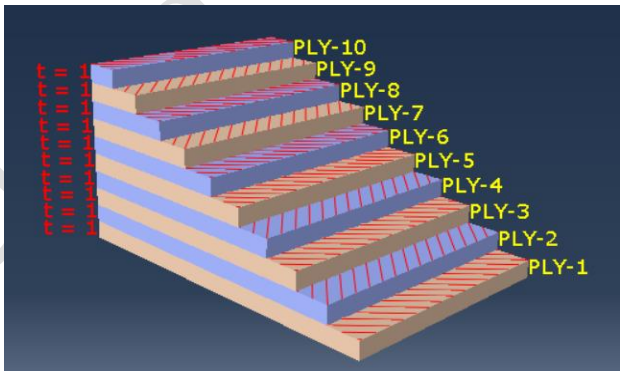

Fig. 4. Laminate configurations

Table 2. Details of laminate configurations and beam geometry

Laminate configurations	b_f (m)	t_f (mm)	L	b_w	t_w

Flange	Web			(mm)	(mm)	(mm)
$[(0/0)_2]_s$,	$[(0/0)_2]_s$,					
$[(\pm45)_2]_s$,	$[(\pm45)_2]_s$,					
$[(90/90)_2]_s$	$[(90/90)_2]_s$	{0.75, 1, 1.25, 1.5}	{1, 1.5, 2}	5000	600	30
$[(0)_2/(\pm45)]_s$	$[(0)_2/(\pm45)]_s$					
$[(0)_2/(90)_2]_s$	$[(0)_2/(90)_2]_s$					

2.2 Validation study

Before analysis, establishing the accuracy of models is essential. Results reported by Upadhyay and Kalyanaraman (2003), Chandak et al. (2008), Qiao and Shan (2005) and Kollar (2003) are used to measure the accuracy of FE modelling. Upadhyay and Kalyanaraman (2003), Chandak et al. (2008) proposed an artificial neural network (ANN)-based approach for predicting the effective width ratio of symmetrical laminated composite box beams, thereby addressing the influence of shear lag in such structural elements. Similarly, Qiao and Shan (2005) and Kollar (2003) have presented local buckling coefficient for the box-beam subjected different lateral loads. To ensure the accuracy of the finite element model, validation was carried out by modeling identical beams in ANSYS to evaluate the effective width ratio and buckling coefficient. The comparison is shown in Table 3 and 4. It shows the compared properties and dimensions of box-beam. The results reported by Upadhyay and Kalyanaraman (2003), Chandak et al. (2008), Qiao and Shan (2005) and Kollar (2003) and present study shows good agreement.

Table 3. Validation of finite element model - Effective width ratio comparison

b_f/b_w	$(b/t)_f$	t_f/t_w	L/b_f	Laminate configurations		Effective width ratio $(b_e/b)_f$	
				Flange	Web	Reference studies	Present studies
4	200	1	5	$[0/0/0]_s$	$[0/0/0]_s$	0.33[a]	0.29
4	200	1	5	$[90/90/90]_s$	$[90/90/90]_s$	0.70[a]	0.68
2.93	122.22	1	5	$[0/0/0]_s$	$[0/0/0]_s$	0.44[b]	0.41
3.61	147.72	0.80	5	$[0/0/0]_s$	$[90/90/90]_s$	0.58[b]	0.54
4	111.11	0.70	5	$[0/0/0]_s$	$[0/0/0]_s$	0.46[b]	0.45

[a]Upadhyay and Kalyanaraman (2003),[b]Chandak et al. (2008)

Table 4. Validation of finite element model - Buckling coefficient comparison

Dimensions in mm	N_{cr} (kN/m)		% Difference ((p-q)/p)*100
$b_w \times b_f \times t_w \times t_f$	FE analysis		
	Reference studies (p)	Present study (q)	
152×152×6.4×6.4	717[c]	758.90	-5.84
152×102×6.4×6.4	850.1[c]	905.76	-6.54
203.2×101.6×6.4×6.4	519[d]	503.47	2.99

[c]Qiao and Shan (2005), [d]Kollar (2003)

2.3 Convergence study

In FE modelling, finer mesh provides more accurate solutions, but it increases the computational time. Hence, to manage the accuracy as well as computing resource herein mesh convergence study is performed. In the present study, several mesh sizes were investigated. The number of elements in flange, web and span length are identified by a code $n_f \times n_w \times n_l$. A convergence test on the beam 1000(b_f)x600(b_w)x5000(L) is performed. The first eigenvalues of five finite element models with increasing mesh refinement are presented in Table 5. The mesh finally adopted is composed of 17 and 15 elements along the flange and web, respectively, and 200 elements along the span length, resulting in 11520 finite elements. Similar studies are carried out for the remaining sections.

Table 5. Mesh Convergence Study

Mesh #	n_f	n_w	n_l	n_{el}	K_f
1	5	5	60	1200	1.8819
2	8	8	100	3200	1.8741
3	12	10	150	6600	1.8725
4	17	15	180	11520	1.8723
5	20	15	200	14000	1.8723

Total number of elements (n_{el}) = $2(n_f+n_w)n_l$

2.4 Buckling mode shape

In all cases, box-beam dimensions are chosen to fail by flange buckling. Web buckling is excluded by providing thicker plates. In each case, buckling takes place at top flange due to compression. Buckling contour plots of the first mode (beam size-750×600×5000) is shown in Fig. 5.

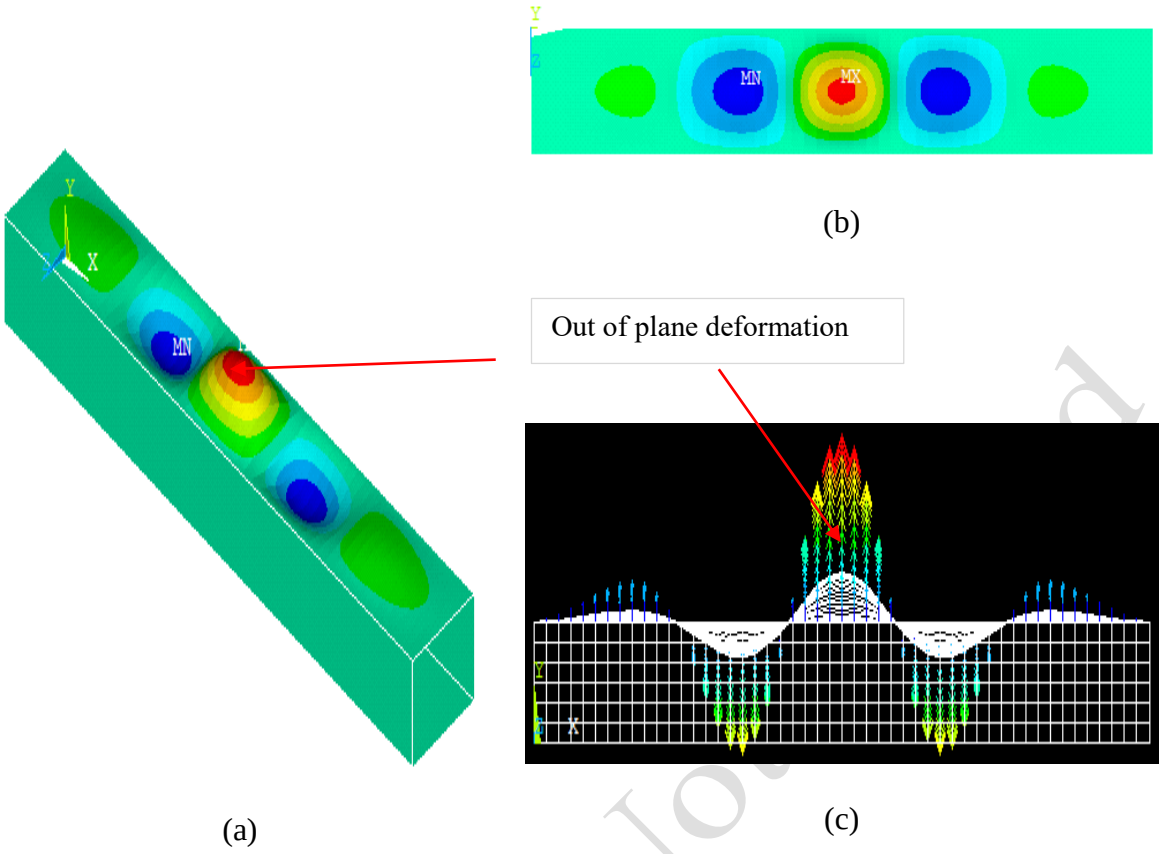

Fig. 5. Buckling contour plots of mode 1: (a) Isometric view, (b) Top view and (c) Side view.

3. Secondary effects

Buckling strength of FRP box beam depends on state of stress in flange and web elements which is influenced by classical effects (compression in top flange and shear in web) and secondary effects (rotational restraint, moment gradient and shear lag). Fig. 6 shows the possible secondary effects in symmetrically loaded box-beams. In this study, to understand the effect of shear lag on flange buckling coefficient the influence of other two secondary effects such as rotational restraint and moment gradient are isolated by choosing appropriate geometry and loading conditions. The procedure used for obtaining shear lag effect on flange buckling coefficient has been described with a flow chart given in Fig. 7.

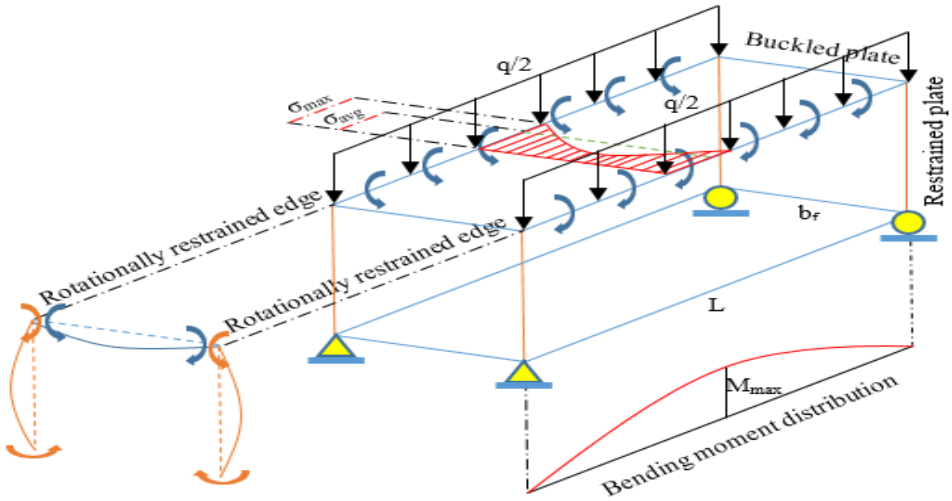

Fig. 6. Structural Representation of a Buckled Plate Segment in a Beam System with Rotational Restraints and bending moment distribution

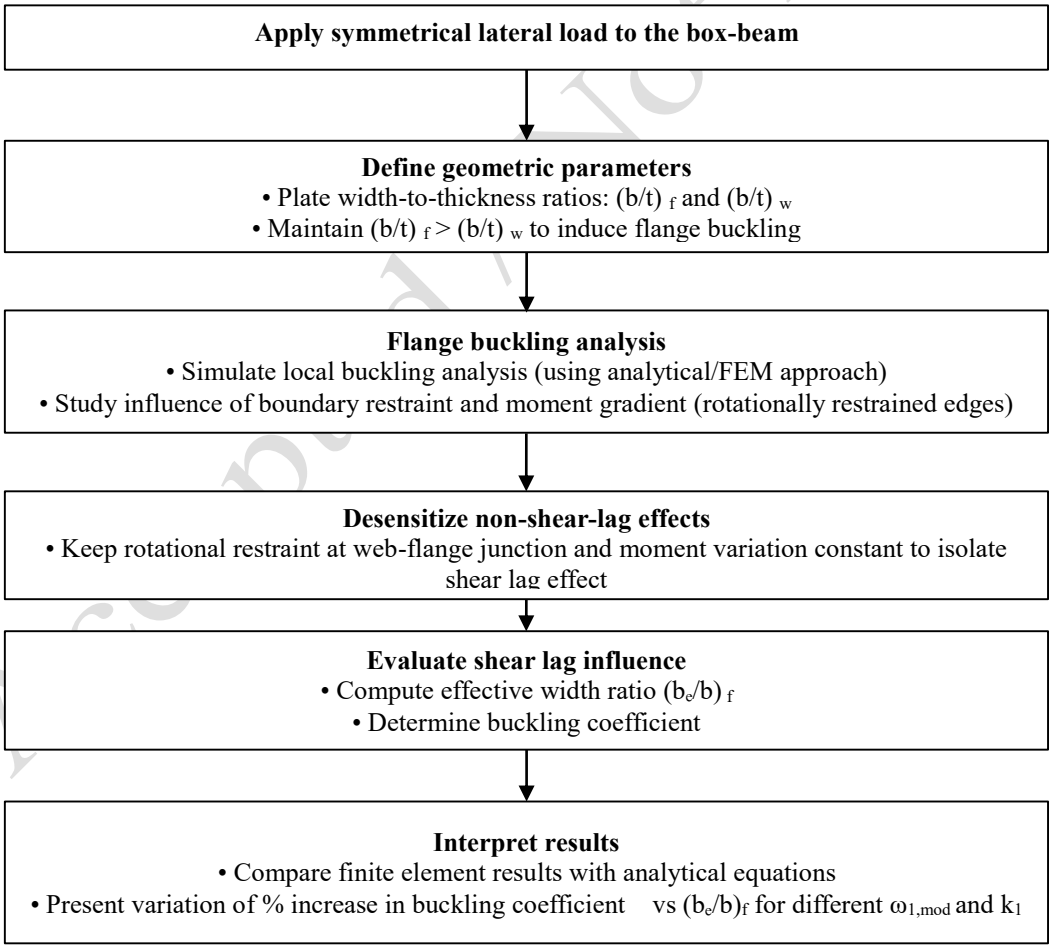

Fig. 7 Flow chart for obtaining effect of shear lag on buckling coefficient

3.1 Desensitization of rotational restraint and moment gradient effect

The effect of rotational restraint and moment gradient on flange buckling was extensively studied by Kasiviswanathan and Upadhyay (2018). From their studies, it can be observed that with an increase in rotational restraint up to a certain value the buckling stress increases rapidly. An increase beyond the limiting value does not further raise the buckling stress. This indicates that as the rotational restraint increases up to a certain level, the boundary condition at the web–flange junction transitions from simply supported to fixed. Once the fixity condition is achieved at web-flange junction further increase in rotational restraint doesn't bring any substantial increase in buckling stress. Hence, in the present work, to isolate the effect of rotational restraint on flange buckling, fixity is achieved at web-flange junction by providing thicker web and high transverse rigidity in webs.

Similarly, to study the effect of moment gradient on flange buckling Kasiviswanathan and Upadhyay (2018) have considered two types of moment cases such as varying and constant moment cases. In both cases they kept the maximum bending moment constant and compared buckling coefficients. They observed that the maximum increase in buckling coefficient due to moment gradient effect is 34.64% that is when moment is varying along the length direction the buckling strength of the beam is increasing considerably with respect to constant moment case. Hence, to isolate this moment gradient effect on flange buckling, in this study constant moment case (four-point load case) is considered. The beam used for the shear lag study is shown in Fig. 8.

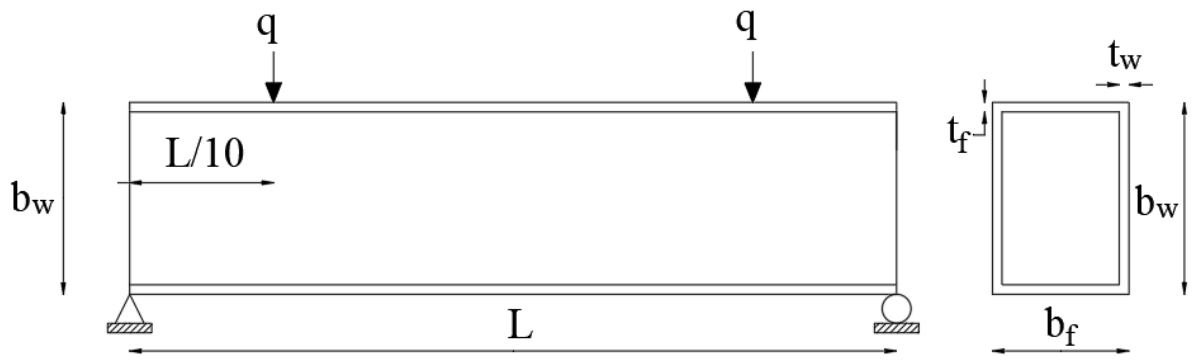

Fig. 8. Schematic view of the beam considered for shear lag study

4. Effect of shear lag on flange buckling

Due to high degrees of orthotropy in FRP beams, the influence of shear lag on stress distribution is high. Further, due to quasi brittle behaviour, no yielding is taking place near ultimate load (which brings uniformity in stress distribution in steel girders) because of this significance of shear lag persists till failure in FRP girders. In view of the above facts, the influence of fiber orientation and geometry (Praseeja and Nithin Mohan (2020) and Kasiviswanathan and Upadhyay (2019)) on shear lag phenomenon as well as influence of shear lag on buckling coefficient needs to be understood for better design.

4.1 Analysis of shear lag effect

In order to evaluate and compare the magnitude of shear lag effect on flange buckling coefficient (K_f) with respect to changes in fiber orientation and geometry the shear lag factor is used. The factor is defined by Eq. (1).

$$SF = \frac{\sigma_{max}}{\sigma_{avg}} \tag{1}$$

Where, the trapezoidal rule of integration is used to calculate the average normal stress (σ_{avg}) and σ_{max} is the maximum normal stress in the beam width (Fig. 1).

4.2 Influence of fiber orientation and geometry on shear lag phenomenon and buckling coefficient

The buckling strength of FRP beam depends on the state of stress and boundary conditions

of the buckling element. State of stress is influenced by the direction of fibers and geometry of the element. Fiber orientation plays a significant role in altering the internal stress distribution within composite structures. For instance, Fig. 9 illustrates the state of stress in the top flange for various combinations of flange–web fiber orientations. Each orientation combination leads to distinct variations in the stress pattern, both along the longitudinal (axial) direction and across the transverse (lateral) direction. This variation arises because the stiffness and load transfer mechanisms of the composite depend strongly on the fiber alignment, thereby influencing how the applied loads are distributed between the flange and web regions. Consequently, even small changes in fiber orientation can cause notable differences in stress magnitude and distribution within the structure.

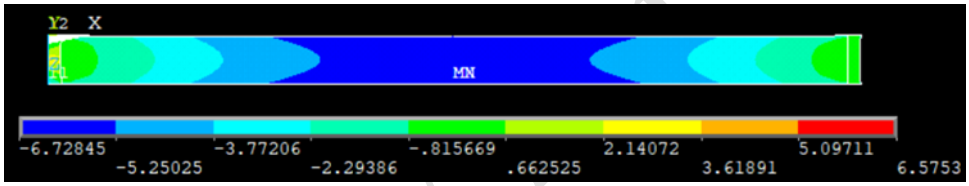

(a)

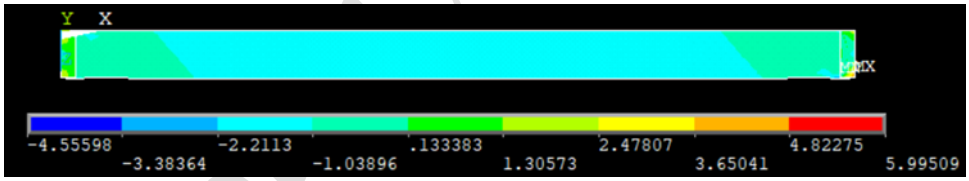

(b)

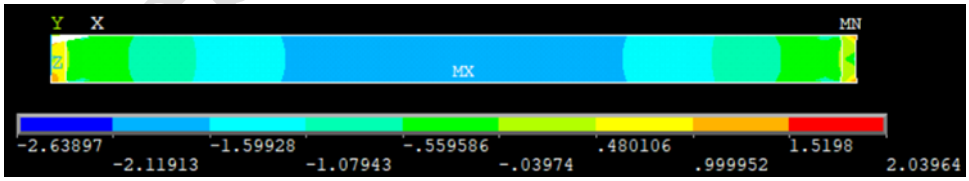

(c)

Fig. 9. State of longitudinal stress on top flange: (a) 0º(θ_f)- 45º(θ_w), (b) ±45º(θ_f)- 45º(θ_w) and (c) 90º(θ_f)- 45º(θ_w).

Further, to show the influence of fiber orientation on shear lag phenomenon, variation of stress across the beam width is presented for three extreme cases of flange fiber orientation such as 0°, ±45° and 90°, while web fiber orientation and geometry of beam are kept constant.

(Kasiviswanathan and Upadhyay (2019) and Praseeja and Nithin Mohan (2020)). Figure 10 shows the longitudinal stress distribution across the top flange at mid-span for different flange–web fiber orientations. In the 0°(θ_f)–±45°(θ_w) configuration [Fig. 10(b)], stresses are highly non-uniform with peak values near the flange–web junction due to strong longitudinal stiffness and shear interaction. For ±45°(θ_f)–±45°(θ_w) [Fig. 10(c)], the stress field becomes more uniform, indicating improved stress transfer and reduced concentration. In the 90°(θ_f)–±45°(θ_w) case [Fig. 10(d)], stresses shift toward the center region with lower magnitudes because the flange fibers, being transverse, contribute less to axial stiffness. Overall, the figure clearly demonstrates that fiber orientation significantly influences the stress magnitude and distribution across the flange width, affecting the load-sharing behavior between flange and web.

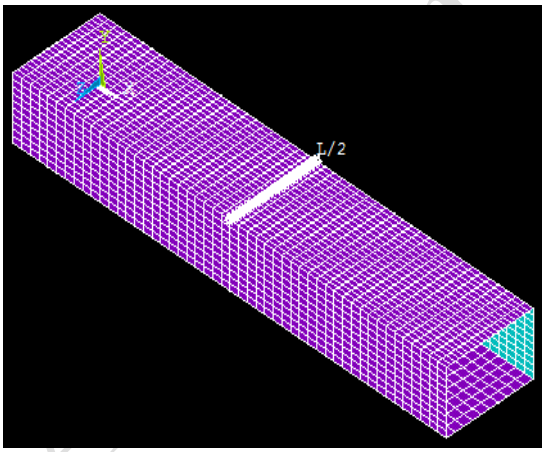

(a)

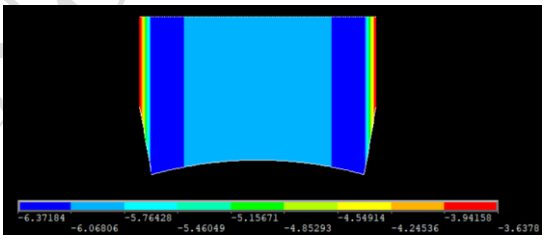

(b)

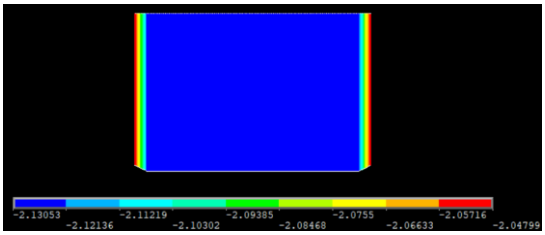

(c)

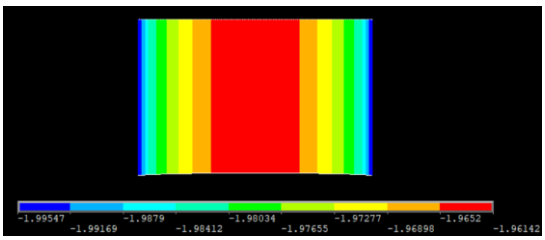

(d)

Fig. 10. Top flange longitudinal stress variation across the beam width: (b) 0º(θ_f) - ±45º(θ_w), (c) ±45º(θ_f) - ±45º(θ_w) and (d) 90º(θ_f) - ±45º(θ_w).

Quantitative information regarding the influence of fiber orientations and geometry on shear lag phenomenon is shown in Fig. 11. Shear lag factors are quantified with help Eq. (1). In Fig. 11 shear lag factors are plotted against different flange width to thickness ratio $(b/t)_f$ for different flange fiber orientations. From this figure, it can be observed that for constant flange fiber orientation, shear lag factor increases with an increase in $(b/t)_f$ that is shear lag increases with increase in ratio of $(b/t)_f$. Further, the figure clearly indicates the effect of flange orthotropy ratio (D_{11}/D_{22}) on the shear lag phenomenon. In general, with increase in degree of orthotropy the shear lag increases but in ±45° case shear lag factors are lower than 0° and 90°. The shear stiffness (A_{66}) of ±45º case is higher than 0° and 90°, it diminishes the stress variation across the beam width (Fig. 10c).

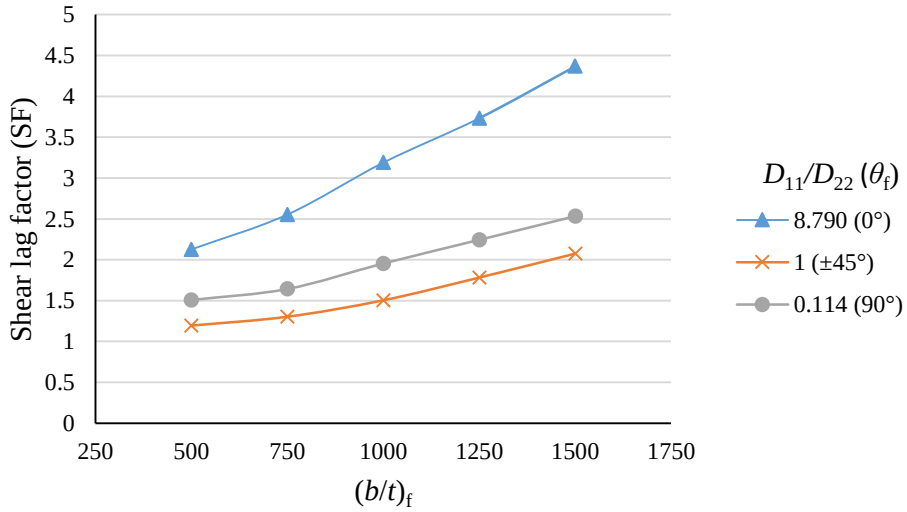

Fig. 11. Influence of fiber orientation and geometry on shear lag phenomenon.

Increase in $(b/t)_f$ ratio, increases shear lag effect as indicated in Fig. 11, but, at the same time increased $(b/t)_f$ decreases buckling coefficient. Separating the effect of $(b/t)_f$ and shear lag on buckling coefficient is intricate. In presence of this coupling, prediction of the real influence of shear lag on buckling coefficient is difficult. Kasiviswanathan and Upadhyay (2019) have attempted to study the effect of shear lag on flange buckling, but they didn't segregate the effect of $(b/t)_f$ on buckling coefficient. Hence, in the present work, to show the effect of shear lag on

flange buckling coefficient percentage increase in buckling coefficient is reported by comparing FE analysis and closed form equation results which are based on uniform stress distribution (across the width). This approach removes the effect of $(b/t)_f$ ratio on buckling coefficient as it is common in both the results (FE analysis and closed form equations).

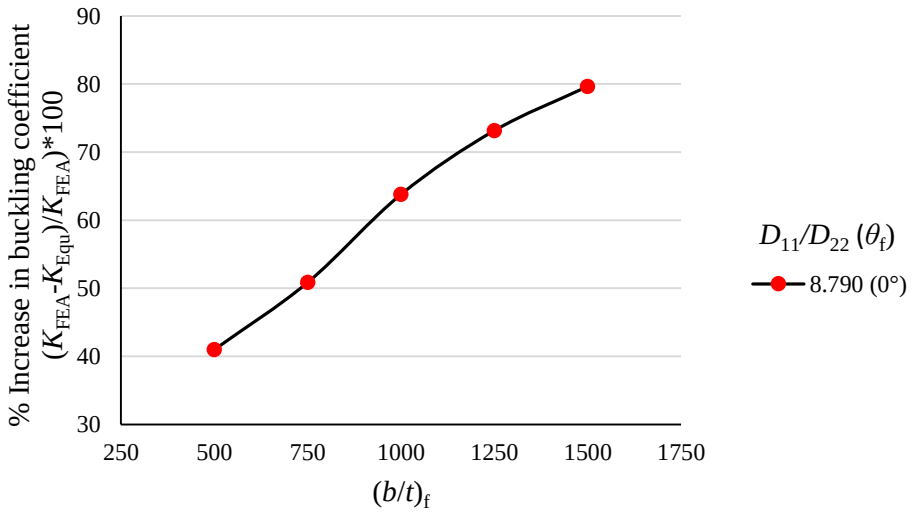

Fig. 12. Influence of shear lag on flange buckling coefficient.

In Fig. 12, percentage increase in buckling coefficient is plotted against different $(b/t)_f$ (the same as adopted in Fig. 9) for 0º flange fiber orientation case to show the influence of shear lag factor (SF) on flange buckling coefficient. It was observed that increasing the section compactness influences the stress distribution within the element and consequently affects the buckling coefficient. To demonstrate this effect, stress variation was analyzed by varying the section compactness. Although an increase in compactness enhances stress variation, it ultimately leads to a reduction in the buckling coefficient. To highlight this behavior, a comparison was made between the finite element analysis results (which consider actual stress variation) and the analytical expressions (based on uniform stress distribution). This comparison clearly illustrates the influence of section compactness on the buckling behavior of the section. The corresponding shear lag factor (SF) for 0º flange fiber orientation also increases with increase in $(b/t)_f$ (Fig. 11), it implies that buckling coefficient increases with

increase in shear lag. Similar behaviour is observed in ±45° and 90° flange fiber orientation cases.

5. Shear lag parameters

The previous section clearly shows the influence of fiber orientation and geometry of box-beams on shear lag phenomenon and flange buckling coefficient. However, the presence of large number of variables due to orthotropy and their inter dependency makes it difficult to understand the effect of shear lag on buckling coefficient. To reduce the variable as well as to understand the effect of shear lag on buckling coefficient, influential parameters need to be identified. On the basis of numerical study, Chandak et al. (2008) have presented two parameters for symmetrically laminated composite box beams i.e. ω_1 and k_1. The parameter ω_1 mainly depends on extensional stiffness to shear stiffness ratio and both flange and web's contribution is considered. In ω_1, web's contribution is taken as, $1/6*(A_{11}/A_{66})_w$ however, it is observed that the coefficient 1/6 is valid only when we are dealing with isotropic material or orthotropic having same axial stiffness in web and flange. Whereas this will not valid when we deal with web and flange elements having different axial stiffnesses due to adoption of different fiber orientations in web and flange as per their specific requirement. In present work based on numerical study results, following modification in webs contribution is suggested. The parameter k_1 depends on axial and flexural stiffness of flange normalized by global axial and flexural stiffness of FRP box-beam. Herein, the parameters $\omega_{1,mod}$ and k_1 are used to quantify the influence of shear lag on flange buckling coefficient. Shear lag phenomenon is quantified by using effective width ratio $(b_e/b)_f$. The parameters are defined as follows.

$$b_{ef} = b_f * \left(\frac{Nominal\ \ bending\ \ stress}{Maximum\ \ bending\ \ stress}\right) \tag{2}$$

$$\omega_1 = \left\{\left(\frac{1}{2}\right)\left(\frac{A_{11}}{A_{66}}\right)_{ft}\right\} + \left\{\left(\frac{1}{6}\right)\left(\frac{A_{11}}{A_{66}}\right)_{w}\right\} \tag{3}$$

$$\omega_{1,mod} = \left\{\left(\frac{1}{2}\right)\left(\frac{A_{11}}{A_{66}}\right)_{ft}\right\} + \left\{\left(\frac{1}{6}\right)\left(\frac{(A_{11})_w}{(A_{66})_{ft}}\right)\left(\frac{A_{11}}{A_{66}}\right)_w\right\} \quad (4)$$

$$k_1 = \left[\frac{(EA)_{ft}}{(EA)_G}\right] + \left[\frac{(D_{11})_{ft}}{(EI)_G}\right] \quad (5)$$

$$(EA)_G = \left[(EA)_{ft} + (EA)_{fb} + (EA)_w\right] \quad (6)$$

Where,

$(EA)_{ft}$, $(EA)_{fb}$ and $(EA)_w$ are the smeared stiffness of top flange, bottom flange and web, respectively and are defined as

$$(EA)_{ft} = (ET)_{ft} \times B \quad (7)$$

$$(EA)_{fb} = (ET)_{fb} \times B \quad (8)$$

$$(EA)_w = (ET)_w \times \left(h - t_{ft} - t_{fb}\right) \times 2 \quad (9)$$

where,

$$(ET)_{ft} = \left[(A_{11})_{ft} - \left\{(A_{12})_{ft} \times (A_{12}/A_{22})_{ft}\right\}\right] \quad (10)$$

$$(ET)_{fb} = \left[(A_{11})_{fb} - \left\{(A_{12})_{fb} \times (A_{12}/A_{22})_{fb}\right\}\right] \quad (11)$$

$$(ET)_w = \left[(A_{11})_w - \left\{(A_{12})_w \times (A_{12}/A_{22})_w\right\}\right] \quad (12)$$

where, $(EI)_G$ is the flexural rigidity of the beam section, $(EI)_{ft}$, $(EI)_{fb}$ and $(EI)_w$ are the flexural rigidities of top flange, bottom flange and web, respectively and are defined as

$$(EI)_G = \left[(EI)_{ft} + (EI)_{fb} + (EI)_w\right] \quad (13)$$

$$(EI)_{ft} = \left[\left\{(D_{11})_{ft} \times B\right\} + \left\{(EA)_{ft} \times \left(n_c - t_{ft}\right)^2\right\}\right] \quad (14)$$

$$(EI)_{fb} = \left[\left\{(D_{11})_{fb} \times B\right\} + \left\{(EA)_{fb} \times \left(D - n_c - t_{fb}\right)^2\right\}\right] \quad (15)$$

$$(EI)_w = \left[\left\{(ET)_w \times \frac{\left(b_w - t_{ft} - t_{fb}\right)^3}{12}\right\} + \left\{(EA)_w \times \left(\frac{\left(b_w - t_{ft} - t_{fb}\right)^2}{2} - n_c - t_{ft}\right)^2\right\}\right] \quad (16)$$

Where, in above equations (2 to 16), *t* and *b* are the thickness and width of the elements and subscripts fb, ft and *w* refer to the bottom flange, top flange and web of the box beams. *A*-

terms refers to the shear and extensional stiffness, and *D*-terms refers to the bending stiffness of the classical laminate plate theory.

The significance of $\omega_{1,mod}$ is shown in Table 6. In this table, values of ω_1, $\omega_{1,mod}$ and $(b_e/b)_f$ are shown for different fiber orientation and geometry. For constant fiber orientation, with respect to changes in geometry $\omega_{1,mod}$ is varying along with $(b_e/b)_f$ but ω_1 is not varying. It shows that the parameter $\omega_{1,mod}$ predicts the effective width ratio more accurately than ω_1. As a result, it is a better parameter than ω_1 and will be useful in prediction the shear lag behaviour in better manner.

Table 6. Significance of modified ω_1

θ_f(Deg)	θ_w (Deg)	t_w/t_f	k_1	ω_1	$\omega_{1,mod}$	$(b_e/b)_f$
0	0	10	0.045	21.822	70.92	0.769
0	0	15	0.031	21.822	98.20	0.619
0	0	20	0.023	21.822	125.48	0.566
±45	±45	10	0.100	0.836	2.72	0.678
±45	±45	15	0.071	0.836	3.76	0.634
±45	±45	20	0.055	0.836	4.81	0.582
90	90	10	0.116	2.483	8.07	0.543
90	90	15	0.083	2.483	11.17	0.491
90	90	20	0.065	2.483	14.28	0.465

6. Effect of shear lag parameters on buckling coefficient

To illustrate the influence of shear lag on the flange buckling coefficient, results are

presented for the same k_1, where the effective width ratio $(b_e/b)_f$ and the percentage difference in the buckling coefficient are compared. These comparisons are made between the finite element analysis outcomes and the analytical results derived from equations based on uniform stress distribution across the flange width, for different values of $\omega_{1,mod}$ (see Fig. 13). Fig. 13(a-c) corresponds to different t_w/t_f ratios. From these figures, it can be noticed that $(b_e/b)_f$ decreases with increase in $\omega_{1,mod}$ and k_1 that is shear lag increases with increase in $\omega_{1,mod}$ and k_1. While, in Fig. 13(d-f) with increase in $\omega_{1,mod}$ and k_1 the percentage difference in buckling coefficient increases. It implies that buckling coefficient increases with increase of shear lag phenomenon. For various values of $\omega_{1,mod}$ and k_1, Table 7 presents the percentage increase in the buckling coefficient corresponding to changes in the top flange stress distribution. The results indicate that when the stress variation in the transverse direction (caused by shear lag) is more pronounced, the percentage increase in the buckling coefficient also becomes higher. Furthermore, based on the numerical results obtained in this study, an attempt has been made to predict the percentage increase in the buckling coefficient due to shear lag for five distinct categories defined by the parameters $\omega_{1,mod}$ and k_1. This data presented in Table 8 will be useful to the designers during the preliminary stages.

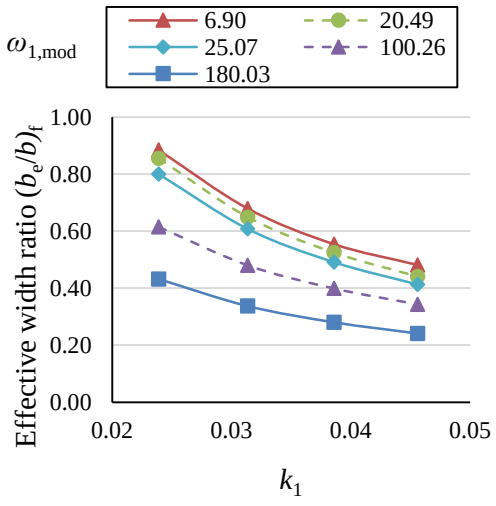

(a)

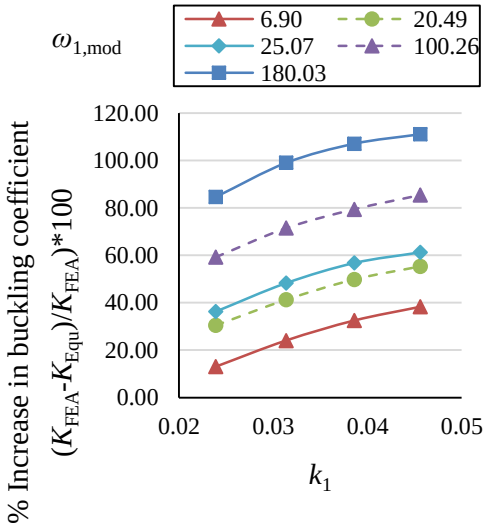

(d)

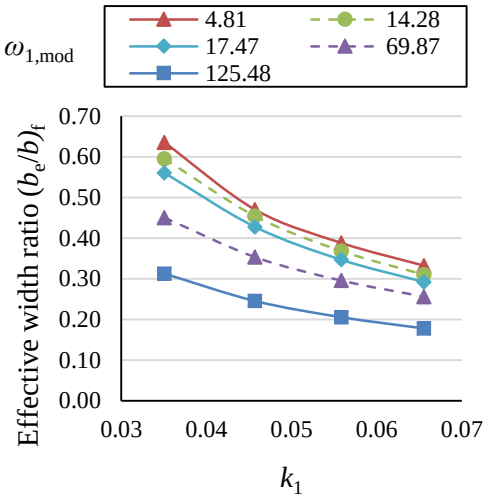

(b)

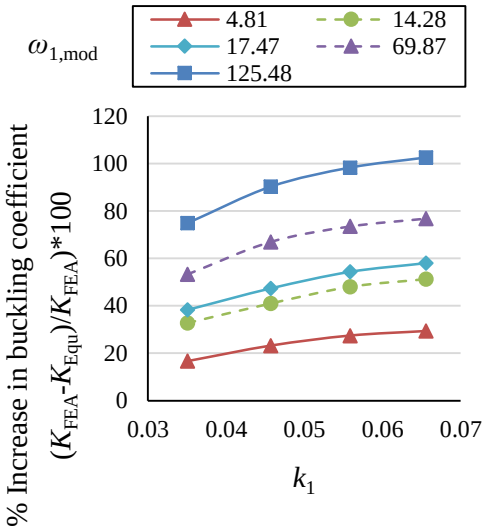

(e)

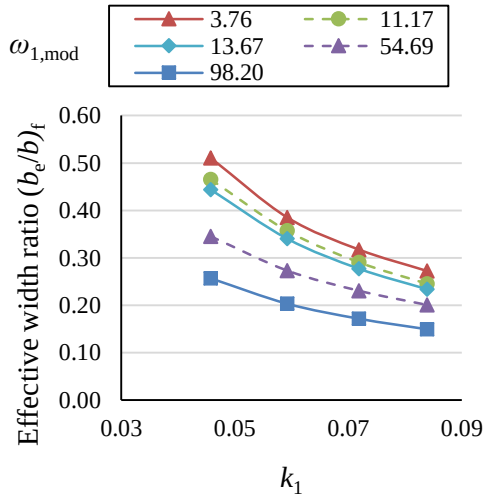

(c)

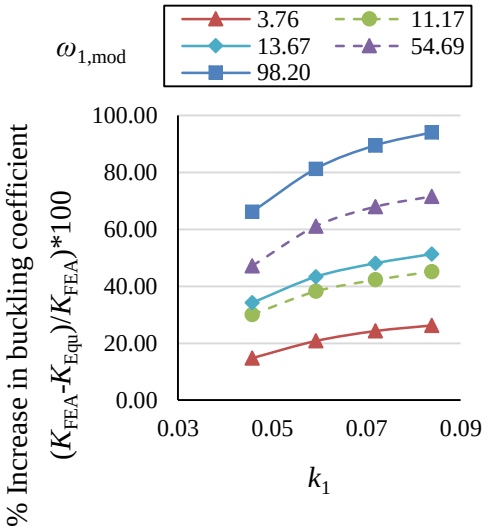

(f)

Fig. 13. Influence of $\omega_{1,mod}$ and k_1 on $(be/b)_f$ and percentage difference in buckling coefficient: (a,d) $t_w/t_f = 30$; (b,e) $t_w/t_f = 20$; (c,f) $t_w/t_f = 15$.

Table 7. Influence of shear lag on buckling coefficient

$\omega_{1,mod}$	k_1	$(b_e/b)_f$	Top flange stress pattern	% Increase in buckling coefficient	Buckling mode shape
180.03	0.023	0.432	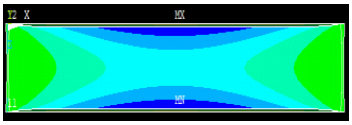	84.53	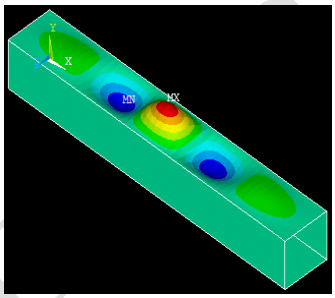
100.26	0.023	0.721	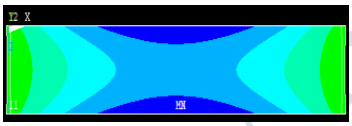	59.25	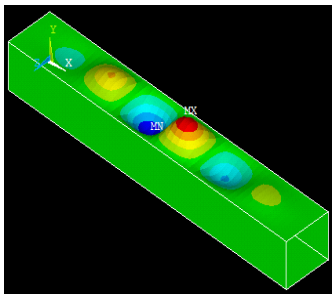
25.07	0.023	0.801	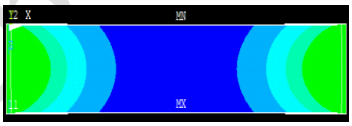	36.23	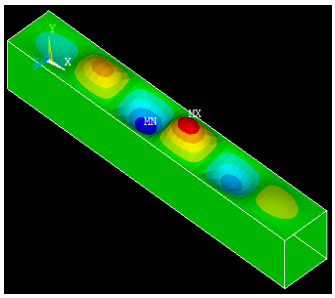
20.49	0.023	0.854	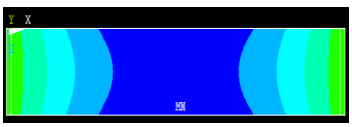	30.49	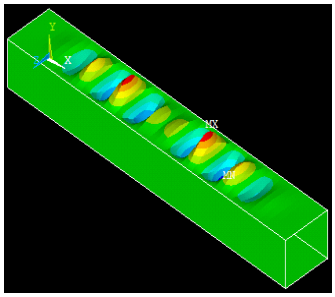

20.49	0.031	0.649	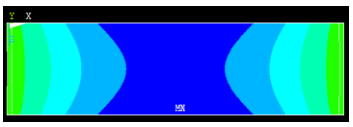	41.23	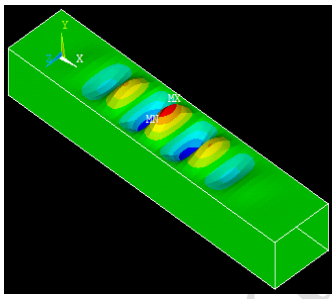
20.49	0.039	0.524	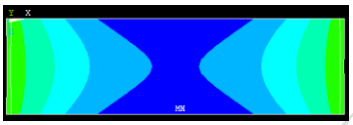	49.77	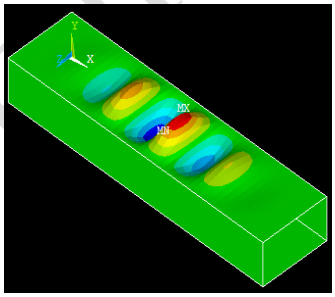
20.49	0.046	0.441	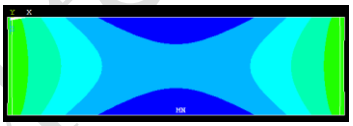	55.23	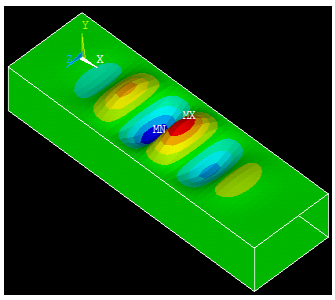
6.90	0.023	0.884	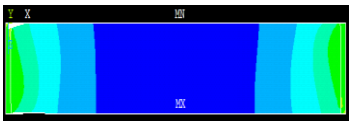	13.01	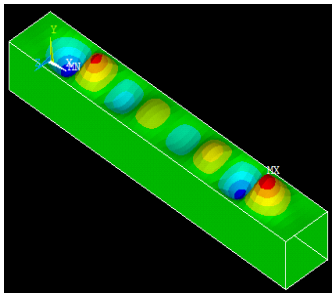

Table 8. % Increase in buckling coefficient based on the present study

	% Increase in buckling coefficient ($(K_{FEA}-K_{Equ})/K_{FEA}$)*100)						
% Increase in buckling coefficient ($(K_{FEA}-K_{Equ})/K_{FEA}$)*100)			$\omega_{1,mod}$				
			Very low (3.5-11.5)	Low (11.5-20.50)	Medium (11.50-70)	High (70-101)	Very high (101-181)
	k_1	Very low (0.01-0.03)	13.01	30.49	36.23	59.25	84.53
		Low (0.03-0.045)	16.70	38.25	53.25	71.43	107.02
		Medium (0.045-0.06)	23.20	43.30	61.58	75.28	111.04
		High (0.06-0.075)	27.42	48.07	67.98	85.28	140.05
		Very high (0.075-0.09)	45.20	51.30	71.61	94.06	160.08

7. Conclusion

Being a thin-walled structure, mostly design of FRP box beam is governed by buckling criterion. Buckling behaviour depends on state of stress in flange and web elements which is influenced by shear lag phenomenon. Further, in the case of composites, shear lag phenomenon becomes more important due to their high degree of orthotropy. Shear lag of composites is

different than steel due to quasi-brittle behaviour as against the typical yielding behaviour of steel which reduces the influence of shear lag at ultimate load. Hence, for better design, the influence of shear lag on buckling coefficient needs to be understood. To bring out the effect of shear lag distinctly, in present study, the effect of rotational restraint and moment gradient on flange buckling is desensitized by selecting appropriate geometry of box beam and loading, respectively. Later, the influence of shear lag on flange buckling coefficient (K_f) of FRP box beams has been studied with the help of modified shear lag parameters $\omega_{1,mod}$ and k_1. Extensive parametric studies through simulations are conducted by changing the geometry and fiber orientation of flange and web elements. Based on the numerical studies carried out in present work and modified shear lag parameters i.e. $\omega_{1,mod}$ and k_1, the following conclusion are drawn, which will be helpful to the design engineers.

- In the present work, two shear lag parameters ω_1 and k_1 are identified and ω_1 is redefined as $\omega_{1,mod}$ to deal with web and flange elements having different axial stiffness.
- Influence of shear lag parameters on effective width ratio $(b_e/b)_f$
    - For constant $\omega_{1,mod}$, effective width ratio $(b_e/b)_f$ decreases with increase in k_1.
    - For constant k_1 effective width ratio $(b_e/b)_f$ decreases with increase in $\omega_{1,mod}$.

  In general, shear lag enhances with increase in parameters $\omega_{1,mod}$ and k_1.
- Influence of shear lag on buckling coefficient
    - Percentage difference in buckling coefficient obtained from non-uniform stress distribution due to shear lag (FEA) and uniform stress distribution by neglecting shear lag (closed form solutions) increases considerably with increase in $\omega_{1,mod}$ and k_1. Indicating that with increase in shear lag buckling coefficient increase considerably.
    - For constant k_1, percentage difference in buckling coefficient is higher for high $\omega_{1,mod}$.

- A table showing % increase in buckling coefficient with shear lag is proposed to help designers.

Based on the present numerical study, it can be observed that buckling coefficient increases with an increase in shear lag and the minimum and maximum increase observed is around 10% to 160%, respectively. The trends coming out of extensive numerical study done in the present work helps to understand the effect of shear lag on flange buckling coefficient as well as shear lag parameters can be used to quantify the effect.

Declaration of Conflict of Interests

The authors declared no potential conflicts of interest with respect to the research, authorship, and/or publication of this article.

Declaration of Competing Interests

The authors declared that they have no known competing for financial interests or personal relationships that could have appeared to influence the work reported in this paper.

References

ANSYS (2003). *User's Manual (Version 15)*, ANSYS Inc., Canonsburg, PA.

Chandak, R., Upadhyay, A. and Bhargava, P. (2008). "Shear lag prediction in symmetrical laminated composite box beams using artificial neural network", *Structural Engineering and Mechanics*, 29(1), 77–89.

Chen, J., Shen, S.L., Yin, Z.Y. and Horpibulsuk, S. (2014). "Closed-form solution for shear lag with derived flange deformation function", *Journal of Constructional Steel Research*, 102, 104–110, https://doi.org/10.1016/j.jcsr.2014.07.003.

Jiang, R., Wu, Q., Xiao, Y., Peng, M., Au, F.T.K., Xu, T. and Chen, X. (2023). "The shear lag effect of composite box girder bridges with corrugated steel webs", *Structures*, 48, 1746–1760, https://doi.org/10.1016/j.istruc.2023.01.108.

Kadhom, M.A., Al-Ansari, L.S. and Gburi, F.H. (2021). "Free vibration analysis of clamped

skew laminated composite plates using ANSYS SHELL281 element", *American Journal of Mechanical Engineering*, 9(1), 33–40.

Kasiviswanathan, M. and Upadhyay, A. (2018). "Flange buckling behaviour of FRP box-beams: A parametric study", *Journal of Reinforced Plastics and Composites*, 37(2), 105–117, https://doi.org/10.1177/0731684417739927.

Kasiviswanathan, M. and Upadhyay, A. (2019). "Effect of shear lag on buckling stress of FRP box-beams", *Recent Advances in Structural Engineering*, 2, 759–770.

Kasiviswanathan, M. and Anbarasu, M. (2021). "Numerical study and design rule for axial capacities of pultruded GFRP hollow columns", *Structures*, 39, 253–265, https://doi.org/10.1016/j.istruc.2021.02.033.

Kilani, A. J., Olubambi, A., Ikotun, B., Onjefu, L. and Abdulwahab, R. (2025). "Predicting the Efficiency of Using Empty Fruit Bunch of Oil-Palm Fibre in Reinforcing Structural Concrete: A Statistical Analysis", *Civil Engineering Infrastructures Journal*, 58(2), 391-417, https://doi.org/10.22059/ceij.2024.365659.1964

Kollar, L.P. (2003). "Local buckling of fiber reinforced plastic composite structural members with open and closed cross sections", *Journal of Structural Engineering*, 129(11), 1503–1513, https://doi.org/10.1061/(ASCE)0733-9445(2003)129:11(1503).

Li, X., Wan, S., Mo, Y.L., Shen, K., Zhou, T. and Nian, Y. (2019). "An improved method for analyzing shear lag in thin-walled box-section beam with arbitrary width of cantilever flange", *Thin-Walled Structures*, 140, 222–235, https://doi.org/10.1016/j.tws.2019.03.025.

Moga, C., Feneşan, C. and Suciu, M. (2020a). "Effective width of steel flange girders related to shear lag phenomenon", *Buletinul Universității Tehnice Gheorghe Asachi*, 66(1), 71–83.

Moga, C., Feneşan, C. and Suciu, M. (2021). "Shear lag and local buckling interaction in orthotropic deck of steel bridges", *Buletinul Universității Tehnice Gheorghe Asachi*, 67(1), 67–79.

Mohammadizadeh, M.R. and Esfandnia, F. (2022). "Predicting compression strength of reinforced concrete columns confined by FRP using meta-heuristic methods", *Civil Engineering Infrastructures Journal*, 55(1), 1–17, https://doi.org/10.22059/ceij.2021.321508.1607.

Nuraliyev, M., Dundar, M.A. and Sahin, D.E. (2022). "Determination of optimal dimensions of polymer-based rectangular hollow sections based on both adequate-strength and local buckling criteria: Analytical and numerical studies", *Mechanics Based Design of Structures and Machines*, 50(6), 1–31, https://doi.org/10.1080/15397734.2021.1910179.

Praseeja, K.C. and Mohan, N. (2020). "Effect of shear lag on buckling behavior of hat-shaped laminated composite box sections", *Proceedings of SECON'19*, Lecture Notes in Civil Engineering, 46, Springer, Singapore, https://doi.org/10.1007/978-981-15-2612-1_34.

Qiao, P. and Shan, L. (2005). "Explicit local buckling analysis and design of fiber-reinforced plastic composite structural shapes", *Composite Structures*, 70(4), 468–483, https://doi.org/10.1016/j.compstruct.2004.09.023.

Said, M., Hassan, M., Rahman, M.A. and Ismail, M. (2022). "Finite element modelling of laminated composite plates using eight-noded SHELL281 element", *International Journal of Integrated Engineering*, 14(4), 198–207, https://doi.org/10.30880/ijie.2022.14.04.021.

Salim, H.A. and Davalos, J.F. (2005). "Shear lag of open and closed thin-walled laminated composite beams", *Journal of Reinforced Plastics and Composites*, 24(7), 673–689, https://doi.org/10.1177/0731684405044607.

Shiyekar, S. and Patil, A. (2023). "Elastic buckling analysis of laminated composite plates using SHELL281 element", *International Journal for Research in Applied Science and Engineering Technology*, 11(5), 245–252.

Si, J., Zeng, Z., Liu, Z., Li, K., Hu, J. and Feng, S. (2023). "Influence of bone joints on the axial compression stability of GFRP hollow cross arms", *Structures*, 47, 374–384,

https://doi.org/10.1016/j.istruc.2022.12.041.

Singh, G.J., Mandal, S., Kumar, R. and Kumar, V. (2020). "Simplified analysis of negative shear lag in laminated composite cantilever beam", *Journal of Aerospace Engineering*, 33(1), 04019103, https://doi.org/10.1061/(ASCE)AS.1943-5525.0001081.

Upadhyay, A. and Kalyanaraman, V. (2003). "Simplified analysis of FRP box-girders", *Composite Structures*, 59, 217–225, https://doi.org/10.1016/S0263-8223(02)00226-7.

Von Kármán, T. (1924). *Strength problems in machine construction*, Encyclopedia of Mathematical Sciences, IV/4, 311–385.

Yamaguchi, E., Chaisomphob, T., Sa-nguanmanasak, J. and Lertsima, C. (2008). "Stress concentration and deflection of simply supported box girder including shear lag effect", *Structural Engineering and Mechanics*, 28(2), 207–220, https://doi.org/10.12989/sem.2008.28.2.207.

Yu, C. and Schafer, B.W. (2007). "Effect of longitudinal stress gradients on elastic buckling of thin plates", *Journal of Engineering Mechanics*, 133(4), 452–463, https://doi.org/10.1061/(ASCE)0733-9399(2007)133:4(452).

Zeinali, E., Nazari, A. and Showkati, H. (2020). "Experimental-numerical study on lateral-torsional buckling of PFRP beams under bending", *Composite Structures*, 237, 111930, https://doi.org/10.1016/j.compstruct.2019.111930.

Nomenclature

L	length of the beam
b_w, b_f	width of the web and flange, respectively
b_e	effective width of the top flange
t_w, t_f	thickness of the web and flange, respectively

N_{cr}	critical load (per unit length)
q	applied loading at the web-flange junction
σ_{max}	maximum bending stress
σ_{avg}	average bending stress
SF	shear lag factor
n_f, $n_{w,}$ n_l	number of elements in the flange, web and beam length, respectively
E_1, E_2, G_{12}	lamina modulus
$\upsilon_{21,}$ υ_{12},	minor and major Poisson's ratio of lamina
$(b_e/b)_f$	effective width ratio
ω_1	orthotropic parameter
$\omega_{1,mod}$	modified orthotropic parameter
k_1	cross sectional parameter
θ_w, θ_f	fiber orientation of web and flange element
K_{FEA}	buckling coefficient obtained from the finite element analysis
K_{Equ}	buckling coefficient obtained from the equation
A_{ij}	extensional stiffness coefficients of the laminate
D_{ij}	bending stiffness coefficients of the laminate
D_{11}/D_{22}	orthotropy ratio of the component (flange and web)
$(EA)_G$	smeared axial rigidity of the beam section

$(EA)_{fb}$, $(EA)_w$ and$(EA)_{ft}$	smeared axial stiffness of bottom flange, web and top flange, respectively
$(EI)_{fb}$, $(EI)_w$ and $(EI)_{ft}$	flexural stiffness of bottom flange, web and top flange, respectively
$(ET)_{fb}$, $(ET)_w$ and $(ET)_{ft}$	smeared extensional stiffness of bottom flange, web and top flange per unit width